J. Korean Inst. Electr. Electron. Mater. Eng.
Vol. 37, No. 5, pp. 547-553 September 2024
doi: https://doi.org/10.4313/JKEM.2024.37.5.12
ISSN 1226-7945(Print), 2288-3258(Online)

Early Stage Report : Graduate Research

# Controlled Synthesis of Colloidal Cu Nanowires and Nanoplates and Their Tunable Localized Surface Plasmon Resonances

**Seokhwan Kim[1,2], Jong Wook Roh[3], Dong Choon Hyun[4], Seonhwa Park[5], and Yuho Min[1,2]**

[1] Department of Materials Science and Metallurgical Engineering, Kyungpook National University, Daegu 41566, Korea
[2] Innovative Semiconductor Education and Research Center for Future Mobility, Kyungpook National University, Daegu 41566, Korea
[3] School of Nano and Materials Science and Engineering, Kyungpook National University, Sangju 37224, Korea
[4] Department of Polymer Science and Engineering, Kyungpook National University, Daegu 41566, Korea
[5] Regional Leading Research Center for Smart Energy System, Kyungpook National University, Daegu 41566, Korea

(Received June 24, 2024; Revised July 22, 2024; Accepted July 23, 2024)

**Abstract:** Precise control over the morphology of nanostructures is critical for tailoring their physical and chemical properties. This study addresses the challenge of developing a simple, integrated method for synthesizing both 1D and 2D colloidal Cu nanostructures in a single system, achieving successful tuning of their localized surface plasmon resonance (LSPR) properties. A facile hydrothermal synthesis utilizing potassium iodide (KI) and hexadecylamine (HDA) is presented for controlling Cu nanostructure morphologies. The key to achieving 1D nanowires (NWs) and 2D nanoplates (NPs) depends on the controlled adsorption of HDA molecules and iodide ($I^-$) ions on specific crystal facets. Depending on the morphologies, the resultant Cu nanostructures exhibit tunable LSPR peaks from 558 nm [nanoplates (NPs)] to 590 nm [nanowires (NWs)]. These results pave the way for the scalable and cost-effective production of plasmonic Cu nanostructures with tunable optical properties, holding promise for applications in sensing, catalysis, and photonic devices.

**Keywords:** Cu nanowires, Cu nanoplates, Localized surface plasmon resonance, Anisotropic growth, Colloidal Cu nanostructures

Control over the morphology of nanostructures is an effective way to tune their physical and chemical properties for target applications [1,2]. Anisotropic nanostructures, particularly those with one-dimensional (1D) and two-dimensional (2D) shapes, have attracted significant interest due to their unique direction-dependent properties, flexibility, and high density of active sites [3]. In particular, metal nanomaterials hold significant potential in diverse fields such as catalysis, plasmonics, spectroscopy, and sensors [4,5]. This stems from their unique physicochemical and surface plasmonic properties. Metal nanomaterials interact with incident electromagnetic waves, leading to the collective oscillation of free electrons under specific conditions, known as localized surface plasmon resonance (LSPR) [6,7]. This occurs when the frequency of the incoming light matches that of the oscillating electrons against the fixed positive nuclei [8]. In this process, metal nanomaterials convert light into a local electric field, producing electromagnetic excitation and massive oscillation of free electrons in metal [9].

For certain metals like Au, Ag, and Cu, LSPR excitation occurs in the visible and near-infrared ranges, depending on their dimension, morphology, and composition. This enables the confinement and tuning of light at the nanoscale [10,11].

✉ **Yuho Min; yuhomin@knu.ac.kr**
**Seonhwa Park; sunhwa2922@knu.ac.kr**

Owing to their unique LSPR characteristics, plasmonic metal nanomaterials have found applications in super lenses [12], quantum computing [13], photochemical lithography [14], Raman-enhanced surface spectroscopy (SERS) [15], and catalysis [16]. Traditionally, research has focused on Ag, Au, and their alloys due to their strong LSPR excitation and the ease of controlling their morphologies to further LSPR optimization. In contrast, Cu nanomaterials have received less attention due to their susceptibility to oxidation and lower LSPR efficiencies. However, their abundance has renewed interest in developing sustainable plasmonic materials [17]. Generally, two distinct strategies have been extensively utilized to prepare Cu nanomaterials free of oxide layers. The first involves removing oxide layers through chemical etching with acids such as HCl and $H_3PO_4$ [18]. The second approach focuses on creating protective coating layers using silver capping, imidazole-based molecules, or organic thiols [19,20].

Among various synthetic methods, solution-based approaches offer significant potential for precise morphology control, large-scale production, and cost-effectiveness [21,22]. Typically, a Cu precursor is reduced by a reducing agent in the presence of an organic surfactant under heating, followed by nucleation and growth into colloidal Cu nanostructures in a liquid solution. To date, 1D Cu nanowires have been successfully prepared using different precursors, surfactants, reducing agents, and solvents [23]. Experimental results have shown that the stronger chemisorption of hexadecylamine (HDA) surfactants on the (100) plane compared to the (111) plane of Cu, in the presence of $Cl^-$ ions at an appropriate concentration, facilitates the anisotropic growth of 1D Cu nanowires through selective atomic attachment on the (111) plane of growing Cu nanocrystals [23,24]. For 2D Cu nanostructures, the initial synthesis of Cu nanodisks involved toxic hydrazine as a reducing agent [25]. Later, researchers improved the aspect ratio using polyvinylpyrrolidone (PVP) polymer and hydrazine in dimethylformamide (DMF) [26]. Subsequently, milder reducing agents were employed in hydrothermal methods to create Cu nanoplates [27]. More recently, Wu *et al.* developed a new approach for Cu nanodisks with better size dispersity and shape yield, although the process is time-consuming (3 days) [28].

Despite the successful development of various approaches to controlling anisotropic colloidal Cu nanostructures, a simple and integrated strategy to induce both 1D and 2D colloidal Cu nanocrystals in one system is still needed. Furthermore, understanding the relationship between LSPR excitation and morphology is crucial for the further application of 1D and 2D Cu nanostructures. Here, we propose a simple synthetic approach to control the formation of both 1D and 2D Cu nanostructures under similar hydrothermal conditions. The key to achieving this morphological variation, from 1D nanowires to 2D nanoplates, lies in the utilization of a potassium iodide (KI) additive. We thoroughly investigated the resultant morphology and crystal structure of 1D and 2D Cu nanocrystals using scanning electron microscopy (SEM; JSM-IT700HR (JEOL)), transmission electron microscopy (TEM; HT-7700 (Hitachi)), atomic force microscopy (AFM; NX20 (Park System)), and X-ray diffractogram (XRD; MiniFlex 600 (Rigaku)) analyses. The LSPR peaks were observed to shift depending on the morphology and dimension, from 590 nm (1D) to 558 nm (2D).

Figure 1 illustrates the schematics of the synthetic protocols for forming 1D and 2D colloidal Cu nanostructures. Both Cu nanowires (NWs) and nanoplates (NPs) were synthesized *via* a hydrothermal reaction. For Cu NWs, copper (II) chloride dihydrate ($CuCl_2{\cdot}2H_2O$, 0.2418 g, Sigma Aldrich), hexadecylamine (HDA, 1.6545 g, Sigma Aldrich) were dissolved in DI water (70 ml), followed by magnetic stirring for 1 h at approximately 25°C. Then, dextrose ($C_6H_{12}O_6$, 0.54059 g, Sigma Aldrich) as a reducing agent was added, and the solution was heated to 40°C in an oil bath under magnetic stirring for 3 h. Subsequently, the light blue aqueous solution was transferred into a Teflon-lined stainless-steel autoclave and heated to 120°C at a heating rate of 5°C/min in a furnace. After 16 h, the reaction batch was allowed to cool down to approximately 25°C. The solution color changed from light blue to reddish-brown, indicating the reduction of Cu precursors to Cu NWs. The final products (1D NWs) were collected three times each by centrifugation (4,500 rpm, 8 min) with DI water, hexene, and ethanol. As previously reported, HDA molecules are strongly adsorbed on the Cu (100) rather than Cu (111) facets under a certain concentration of $Cl^-$ ions, which stabilize the (100) planes and promote the anisotropic growth by attaching Cu atoms onto the (111) [23]. The same growth mechanism for Cu nanowires can be applied in this study.

2D Cu NPs were synthesized using the same experimental procedure as for Cu NWs, except for the addition of a specific

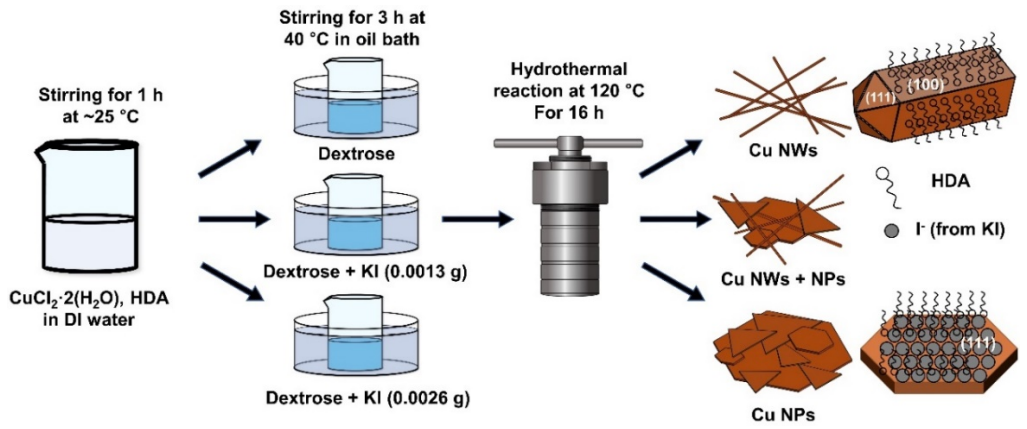


**Fig. 1.** Schematic illustration of the experimental procedure for synthesizing 1D and 2D Cu nanostructures, showing the possible adsorption of HDA and $I^-$ on (100) and (111) planes, respectively.

concentration (e.g., molar ratio) of potassium iodide (KI, Sigma Aldrich) at the step when dextrose was introduced. To understand the effect of KI, different concentrations (0.0013 g and 0.0026 g) were added. In both cases, the final products were Cu NPs with triangular and hexagonal morphologies. However, the presence of trace amounts of Cu NWs in the final products was obtained when using a relatively low concentration of KI (0.0013 g), suggesting that KI plays a key role in morphological variation from 1D to 2D nanostructures. Interestingly, using the same molar amount of Iodine ($I_2$) instead of KI under the same conditions also yielded 2D Cu nanoplates (not shown here). Therefore, we propose that $I^-$ ions selectively adhere to the (111) facets, the basal planes of Cu nanoplates (further discussion on lattice planes will be included in the following TEM analysis part), possibly leading to anisotropic plate-like growth. When the concentration of $I^-$ ions is insufficient, as in the case of using 0.0013 g of KI in this study, (111) facets of some Cu nanocrystals might not be fully adhered by $I^-$ ions, which grow further into NWs instead of NPs. The exact configuration and experimental evidence for the selective adsorption of $I^-$ on (111) facets require further investigation with theoretical calculations, which will be conducted in another study.

The overall morphologies and dimensions of the synthesized Cu nanostructures were investigated using SEM images (Fig. 2). Figure 2(a) shows a typical SEM image of Cu NWs with diameters and lengths ranging from 35 to 72 nm and from 40 to 50 μm, respectively. The inset in Fig. 2(a) exhibits the pentagonal edge, indicating that the growth of Cu NWs started from five-twined pentagonal seed particles *via* self-seeded growth as previously reported [29]. During this self-seeded growth, HDA molecules selectively adsorbed on the (100) planes of growing nanocrystals, stabilizing those planes and promoting preferential atomic attachment toward the (111) planes for anisotropic 1D growth. Adding KI to the aqueous solution and subsequent hydrothermal reaction yielded 2D Cu NPs with hexagonal and triangle shapes [Figs. 2(b), (c)]. The lateral dimension of Cu NPs ranges from sub-micron to several tens micrometers in both cases. Their ultrathin nature is evident where two or more NPs overlap, revealing the bottom NPs. While HDA molecules play a key role in the formation of pentagonal seeds and subsequent 1D NWs, they are only weakly adsorbed on the Cu, making them ineffective for the growth of Cu NPs [30]. When KI is added, $I^-$ ions can be adsorbed on the (111) planes, hindering the growth of (111) and resulting in the formation of 2D NPs. Similar experimental results were recently reported, where iodine was shown to regulate the growth of 2D Cu NPs through the adsorption on the (111) facets [27,30]. In our study, reducing the concentration of KI resulted in small amounts of NWs in the final product, indicating that the adsorption of HDA is relatively unfavorable compared to $I^-$ ions on Cu nanostructures. The crystal structure of the Cu nanostructures was confirmed by XRD analysis [Fig. 2(d)]. Three characteristic peaks corresponding to the (111), (200), and (220) planes indicate the face-centered cubic phase (JCPDS# 04-836). In addition, the absence of secondary Cu oxide peaks confirms the high purity of the Cu nanostructures.

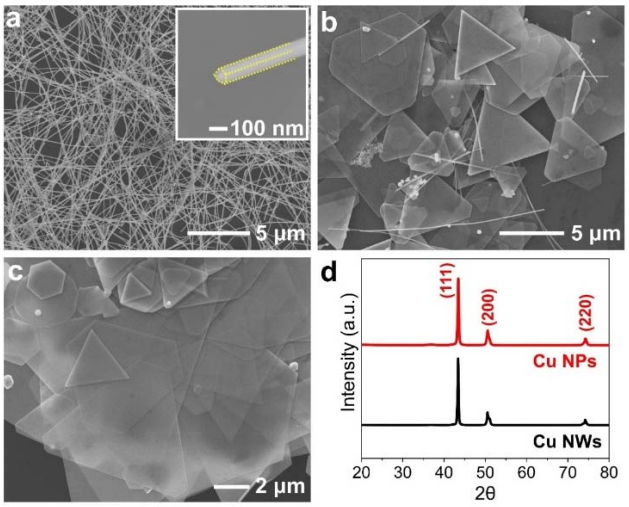


**Fig. 2.** (a-c) Scanning electron microscopy (SEM) images of Cu (a) nanowires (NWs), (b) nanoplates (NPs) with some NWs, and (c) nanoplates (NPs) synthesized with varying concentrations of KI: no KI, 0.0013 g of KI, and 0.0026 g of KI, respectively [the inset of Fig. 2(a) shows a high-magnification SEM image highlighting the diameter and edge of the Cu NWs]. (d) X-ray diffractograms (XRD) of the as-synthesized Cu NWs (black) and Cu NPs (red).

To further understand the growing crystal lattice planes of Cu NWs and NPs, TEM analysis was conducted (Fig. 3). Figure 3a and b show low-magnification TEM images of a Cu NW with a diameter of approximately 72 nm. Careful observation of the HR-TEM image [Fig. 3(c)] and corresponding SAED pattern [Fig. 3(d)] reveals that the NW grew along the [110] direction. Furthermore, the SAED pattern shows two superimposed zone axes of [$\bar{1}$12] and [001] of face-centered cubic pattern, which corresponds to previous reports for penta-twined Cu NWs [29]. This indicates that our NW is composed of five sub-crystals [denoted as 1, 2, 3, 4, and 5 in the inset of panel (a)], which share the same <110> axes and are enclosed by {100} side planes and {111} end planes, respectively. In our Cu NW, the superimposed [001] and [$\bar{1}$12] zone axes could be observed when the electron beam is perpendicular to the one side surface of NW as illustrated in the inset of panel (a). Under this orientation, [001] and [ $\bar{1}$ 12] zones are generated from #1 sub-crystal and #2/#3 sub-crystals, respectively. Therefore, the Cu NW possesses penta-twined fivefold symmetric sub-crystals elongating parallel to the twin

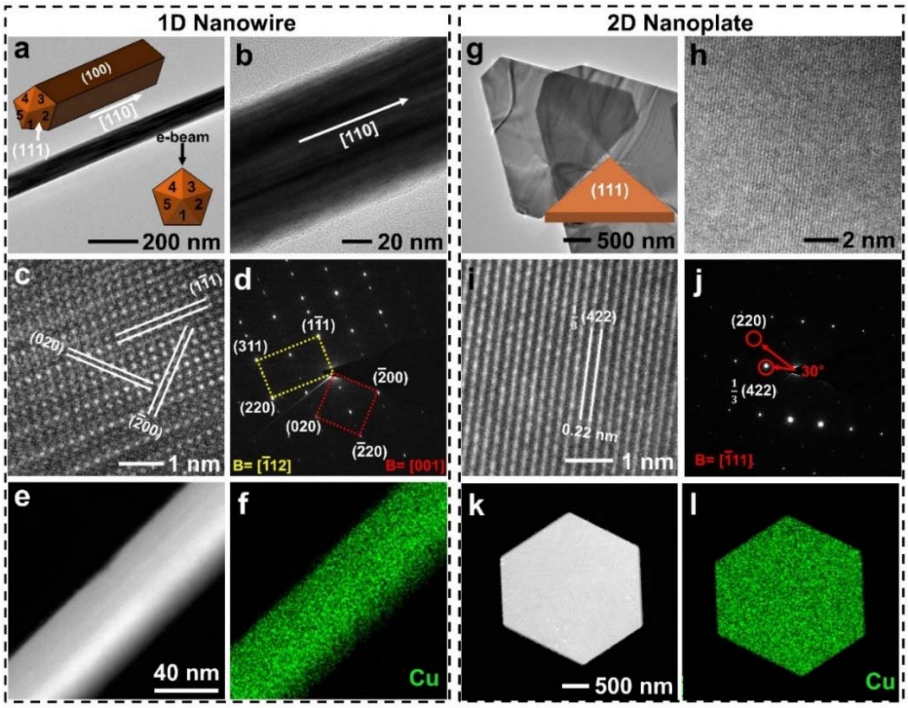


**Fig. 3.** Low-and high-magnification transmission electron microscopy (TEM) images of (a-c) Cu nanowires and (g-i) Cu nanoplates. Selective electron diffraction pattern (SAED) of (d) Cu nanowire and (j) Cu nanoplate obtained from each panel of (c) and (i), respectively. High-angle annular dark field scanning transmission electron microscopy (HAADF-STEM) and corresponding energy dispersive X-ray spectroscopy (EDS) mapping images of (e,f) Cu nanowire and (k,l) Cu nanoplate.

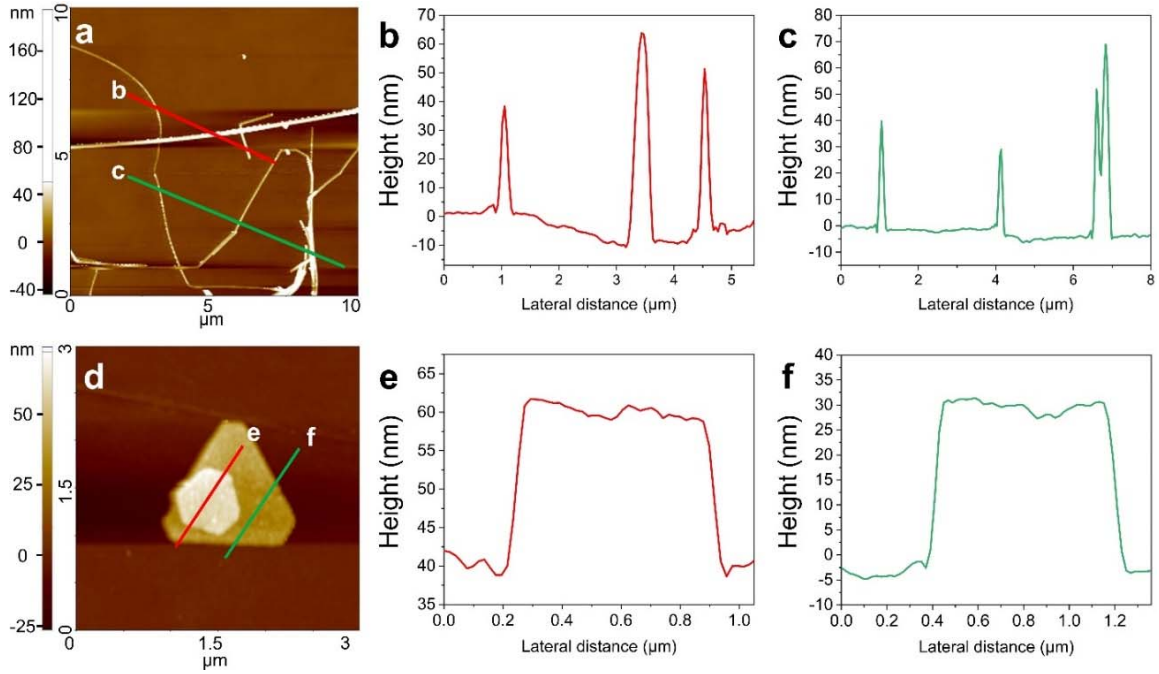


**Fig. 4.** (a) Typical AFM image of Cu nanowires. (b,c) Thickness distributions of Cu nanowires obtained from panel (a) along two directions: (b) red and (c) green lines. (d) AFM image of Cu nanoplates and (e,f) corresponding thickness variations along two directions: (e) red and (f) green lines.

planes, which is consistent with the results for 1D metal nanowires/nanorods grown from pentagonal seeds [31]. The HAADF-STEM image [Fig. 3(e)] and corresponding elemental mapping image [Fig. 3(f)] clearly show the uniform distribution of elemental Cu throughout the Cu NW.

For Cu NP, Fig. 3(g) shows the low-magnification TEM image of a truncated triangle-shaped Cu NP with a lateral dimension of about 2.5 μm. High-magnification TEM images [Figs. 3(h) and (i)] reveal the lattice fringe of 0.22 nm, corresponding to the 1/3(422) reflections of the face-centered cubic structure in the [111] orientation [25]. Indexing the SAED pattern [Fig. 3(j)] obtained from Fig. 3(i) confirms the full orientation of the Cu NP. Two diffraction spots for (220) and 1/3(422) were observed with a 30° angle between them, confirming that Cu NP has (111) basal planes as top and bottom surfaces. While 1/3{422} reflections are generally forbidden for a perfect face-centered cubic crystal, they have been reported to appear when stacking faults are formed within 2D nanostructures [17,32]. HADDF-STEM [Fig. 3(k)] and corresponding EDS mapping [Fig. 3(l)] images show the hexagonal Cu NP and uniform distribution of the Cu element within the 2D nanostructure [Figs. 3(k), (l)].

AFM was conducted to measure the diameter and thickness of Cu NWs and NPs. Figure 4(a) shows a typical AFM image of Cu NWs with two scanning directions denoted by red and green lines. Based on the red line, the thickness was measured as 41, 63, and 55 nm from three different NWs [Fig. 4(b)]. Additionally, we obtained the thicknesses of 42, 34, 57, and 71 nm from four different NWs along the green line [Fig. 4(c)]. The average thickness of NWs, measured along both lines, is approximately 52 nm, which is consistent with the results from SEM images. For 2D Cu NPs, the AFM image exhibits two NPs stacked face-to-face, with the NPs possessing distinct hexagonal and triangular shapes [Fig. 4(d)]. When we scanned the probe along the red line, where the two NPs are stacked, the thickness was found to be about 60 nm [Fig. 4(e)]. When the single NP was scanned along the green line, a thickness of about 30 nm was measured [Fig. 4(f)]. This indicates that each NP possesses a thickness of about 30 nm, suggesting a relatively uniform thickness. The resulting diameter and thickness of these Cu nanostructures are capable of influencing the LSPR properties [6,7], thereby enabling efficient manipulation of light at the nanoscale.

Plasmonic Cu nanostructures exhibit exceptional light

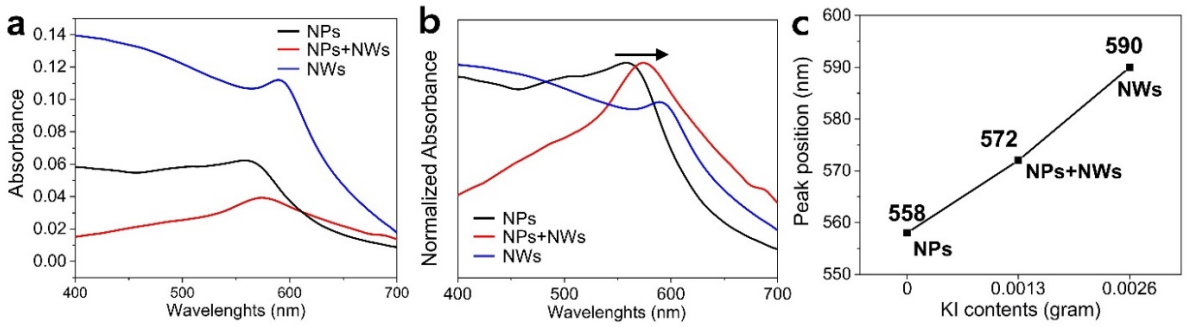


**Fig. 5.** (a) LSPR absorption and (b) normalized absorption spectra of Cu nanostructures hydrothermally synthesized using different amounts of KI: (i) Blue (NWs, 0 g of KI), (ii) Red (mixture of NPs and NWs, 0.0013 g of KI), and (iii) black spectrum (NPs, 0.0026 g of KI). (c) Change in LSPR peak position of the corresponding nanostructures.

manipulation capabilities through the LSPR effect, where the resonance properties can be tuned by factors such as carrier density, morphology, and size [33,34]. Anisotropic morphologies, such as 1D and 2D nanomaterials, exhibit multiple LSPR modes due to their unique geometries. For example, 1D Au nanorods display LSPR band-splitting into transverse and longitudinal modes, where increasing the aspect ratio of Au nanorods results in a red-shift of the longitudinal LSPR mode, while the transverse mode remains within visible ranges [35]. In 2D plasmonic materials, two LSPR modes, specifically low-energy in-plane and high-energy out-of-plane modes, can be observed [36]. An Increase in the aspect ratio shifts the in-plane and out-of-plane LSPR peaks to higher and lower wavelengths, respectively [36]. For 1D and 2D plasmonic nanostructures, longitudinal and in-plane LSPR modes do not develop at high aspect ratios with length or lateral dimensions exceeding several hundred nanometers. In this study, because Cu NWs and NPs possess high aspect ratios (360~600 for NWs, 200~400 for NPs), resulting in only one LSPR band, which can be assigned to transverse LSPR peak for NWs and out-of-plane LSPR peak for NPs. The corresponding UV-visible absorption spectra of as-synthesized Cu nanostructures are shown in Fig. 5(a). The LSPR peaks are centered at 558, 572, and 590 nm for Cu NPs, the mixture (NPs and NWs), and NWs, respectively. The LSPR peak observed in the mixture of NWs and NPs lies between those of pure NWs and NPs, possibly due to the combination of each LSPR peak from NWs and NPs. The red shift of the LSPR peaks from 558 nm (for NPs) to 590 nm (for NWs), depending on their morphologies [Figs. 5(b), (c)], highlights the tunability of LSPR properties by controlling morphologies of Cu nanostructures.

In conclusion, this work presents a facile hydrothermal method for synthesizing Cu nanostructures with tunable morphologies and LSPR properties. The key to achieving 1D nanowires (NWs) and 2D nanoplates (NPs) lies in the controlled adsorption of HDA molecules (hexadecylamine) and iodide ($I^-$) ions on specific crystal facets. The LSPR peak position varied from 558 nm (NPs) to 590 nm (NWs), demonstrating successful morphology-dependent tunability of light response.

## ORCID

Yuho Min https://orcid.org/0000-0002-0784-4818
Seonhwa Park https://orcid.org/0000-0001-9544-6651

## ACKNOWLEDGEMENTS

This work was supported by the National Research Foundation of Korea (NRF) grant funded by the Ministry of Science and ICT (2021R1A5A8033165 and RS-2023-00241159).

## REFERENCES

[1] Y. Min, G. D. Moon, C. E. Kim, J. H. Lee, H. Yang, A. Soon, and U. Jeong, *J. Mater. Chem. C*, **2**, 6222 (2014). doi: https://doi.org/10.1039/C4TC00586D

[2] T. H. Yang, Y. Shi, A. Janssen, and Y. Xia, *Angew. Chem. Int. Ed.*, **59**, 15378 (2020). doi: https://doi.org/10.1002/anie.201911135

[3] A. K. Pearce, T. R. Wilks, M. C. Arno, and R. K. O'Reilly, *Nat. Rev. Chem.*, **5**, 21 (2021).
doi: https://doi.org/10.1038/s41570-020-00232-7

[4] Y. Y. Cai, Y. C. Choi, and C. R. Kagan, *Adv. Mater.*, **35**, 2108104 (2023).
doi: https://doi.org/10.1002/adma.202108104

[5] X. Ma, H. Sun, Y. Wang, X. Wu, and J. Zhang, *Nano Energy*, **53**, 932 (2018).
doi: https://doi.org/10.1016/j.nanoen.2018.09.042

[6] M. L. Brongersma, N. J. Halas, and P. Nordlander, *Nat. Nanotechnol.*, **10**, 25 (2015).
doi: https://doi.org/10.1038/nnano.2014.311

[7] Y. Zhang, S. He, W. Guo, Y. Hu, J. Huang, J. R. Mulcahy, and W. D. Wei, *Chem. Rev.*, **118**, 2927 (2018).
doi: https://doi.org/10.1021/acs.chemrev.7b00430

[8] S. Linic, U. Aslam, C. Boerigter, and M. Morabito, *Nat. Mater.*, **14**, 567 (2015).
doi: https://doi.org/10.1038/nmat4281

[9] N. Jiang, X. Zhuo, and J. Wang, *Chem. Rev.*, **118**, 3054 (2018).
doi: https://doi.org/10.1021/acs.chemrev.7b00252

[10] Y. Min, H. J. Seo, J. J. Choi, B. D. Hahn, and G. D. Moon, *Nanotechnology*, **29**, 345603 (2018).
doi: https://doi.org/10.1088/1361-6528/aac929

[11] T. P. Araujo, J. Quiroz, E.C.M. Barbosa, and P.H.C. Camargo, *Curr. Opin. Colloid Interface Sci.*, **39**, 110 (2019).
doi: https://doi.org/10.1016/j.cocis.2019.01.014

[12] S. Kawata, Y. Inouye, and P. Verma, *Nat. Photonics*, **3**, 388 (2009).
doi: https://doi.org/10.1038/nphoton.2009.111

[13] J. Lee, D. J. Jeon, and J. S. Yeo, *Adv. Mater.*, **33**, 2006606 (2021).
doi: https://doi.org/10.1002/adma.202006606

[14] Z. Wang, B. Ai, H. Möhwald, and G. Zhang, *Adv. Opt. Mater.*, **6**, 1800402 (2018).
doi: https://doi.org/10.1002/adom.201800402

[15] G. Demirel, H. Usta, M. Yilmaz, M. Celik, H. A. Alidagi, and F. Buyukserin, *J. Mater. Chem. C*, **6**, 5314 (2018).
doi: https://doi.org/10.1039/C8TC01168K

[16] U. Aslam, V. G. Rao, S. Chavez, and S. Linic, *Nat. Catal.*, **1**, 656 (2018).
doi: https://doi.org/10.1038/s41929-018-0138-x

[17] L. Scarabelli, M. Sun, X. Zhuo, S. Yoo, J. E. Millstone, M. R. Jones, and L. M. Liz-Marzán, *Chem. Rev.*, **123**, 3493 (2023).
doi: https://doi.org/10.1021/acs.chemrev.3c00033

[18] K. Y. Shin, J. S. Lee, J. Y. Hong, and J. Jang, *Chem. Commun.*, **50**, 3093 (2014).
doi: https://doi.org/10.1039/C3CC49782H

[19] C. K. Kim, G. J. Lee, M. K. Lee, and C. K. Rhee, *Powder Technol.*, **263**, 1 (2014).
doi: https://doi.org/10.1016/j.powtec.2014.04.064

[20] S. Hong, C. Liu, S. Hao, W. Fu, J. Peng, B. Wu, and N. Zheng, *npj Flexible Electron.*, **6**, 17 (2022).
doi: https://doi.org/10.1038/s41528-022-00151-1

[21] Y. Min, J. Kwak, A. Soon, and U. Jeong, *Acc. Chem. Res.*, **47**, 2887 (2014).
doi: https://doi.org/10.1021/ar500133w

[22] Y. Min, E. Im, G. T. Hwang, J. W. Kim, C. W. Ahn, J. J. Choi, B. D. Hahn, J. H. Choi, W. H. Yoon, D. S. Park, D. C. Hyun, and G. D. Moon, *Nano Res.*, **12**, 1750 (2019).
doi: https://doi.org/10.1007/s12274-019-2432-6

[23] J. A. da Silva, M. R. Meneghetti, and P. A. Netz, *ACS Appl. Nano Mater.*, **3**, 5343 (2020).
doi: https://doi.org/10.1021/acsanm.0c00708

[24] M. J. Kim, S. Alvarez, Z. Chen, K. A. Fichthorn, and B. J. Wiley, *J. Am. Chem. Soc.*, **140**, 14740 (2018).
doi: https://doi.org/10.1021/jacs.8b08053

[25] C. Slazemann, J. Urban, I. Lisiecki, and M. P. Pileni, *Adv. Funct. Mater.*, **15**, 1277 (2005).
doi: https://doi.org/10.1002/adfm.200400594

[26] I. Pastoriza-Santos, A. Sánchez-Iglesias, B. Rodríguez-González, and L. M. Liz-Marzán, *Small*, **5**, 440 (2009).
doi: https://doi.org/10.1002/smll.200801088

[27] J. W. Lee, J. Han, D. S. Lee, S. Bae, S. H. Lee, S. K. Lee, B. J. Moon, C. J. Choi, G. Wang, and T. W. Kim, *Small*, **14**, 1703312 (2018).
doi: https://doi.org/10.1002/smll.201703312

[28] K. Wu, C. Sun, Z. Wang, Q. Song, X. Bai, X. Yu, Q. Li, Z. Wang, H. Zhang, J. Zhang, X. Tong, Y. Liang, A. Khosla, and Z. Zhao, *ACS Materials Lett.*, **4**, 650 (2022).
doi: https://doi.org/10.1021/acsmaterialslett.2c00149

[29] H. J. Yang, S. Y. He, and H. Y. Tuan, *Langmuir*, **30**, 602 (2014).
doi: https://doi.org/10.1021/la4036198

[30] A. Sheng, S. Khuje, J. Yu, T. Parker, J. Y. Tsai, L. An, Y. Huang, Z. Li, C. G. Zhuang, L. Kester, Q. Yan, and S. Ren, *ACS Appl. Nano Mater.*, **5**, 4028 (2022).
doi: https://doi.org/10.1021/acsanm.2c00019

[31] C. Lofton and W. Sigmund, *Adv. Funct. Mater.*, **15**, 1197 (2005).
doi: https://doi.org/10.1002/adfm.200400091

[32] V. Germain, J.L.D. Ingert, Z. L. Wang, and M. P. Pileni, *J. Phys. Chem. B*, **107**, 8717 (2003).
doi: https://doi.org/10.1021/jp0303826

[33] Z. Lyu, Y. Shang, and Y. Xia, *Acc. Mater. Res.*, **3**, 1137 (2022).
doi: https://doi.org/10.1021/accountsmr.2c00134

[34] Y. Min, H. J. Seo, J. J. Choi, B. D. Hahn, and G. D. Moon, *Nanotechnology*, **29**, 345603 (2018).
doi: https://doi.org/10.1088/1361-6528/aac929

[35] H. Chen, L. Shao, Q. Li, and J. Wang, *Chem. Soc. Rev.*, **42**, 2679 (2013).
doi: https://doi.org/10.1039/C2CS35367A

[36] N. Kapuria, N. N. Patil, K. M. Ryan, and S. Singh, *Nanoscale*, **14**, 2885 (2022).
doi: https://doi.org/10.1039/D1NR06990J